Two-Phase Flow Patterns in Turbulent Flow Through a Dose Diffusion Pipe

H. Tang, L.C. Wrobel*, I.E. Barton

School of Engineering and Design, Brunel University, Uxbridge, Middlesex, UB8 3PH, UK

Abstract

A numerical investigation is carried out for turbulent particle-laden flow through a dose diffusion pipe for a model reactor system. A Lagrangian Stochastic Monte-Carlo particle-tracking approach and the averaged Reynolds equations with a k-ε turbulence model, with a two-layer zonal method in the boundary layer, are used for the disperse and continuous phases. The flow patterns coupled with the particle dynamics are predicted. It is observed that the coupling of the continuous phase with the particle dynamics is important in this case. It was found that the geometry of the throat significantly influences the particle distribution, flow patterns and length of the recirculation region. The accuracy of the simulations depends on the numerical prediction and correction of the fluid phase velocity during a characteristic time interval of the particles. A numerical solution strategy for the computation of two-way momentum coupled flow is discussed. The three test cases show different flow features in the formation of a recirculation region behind the throat. The method will be useful for the qualitative analysis of conceptual designs and their optimisation.

Key words: two-phase flows, stochastic particle tracking, turbulence, dose diffusion pipe

Nomenclature

Abbreviations

AMG	algebraic multigrid
CFD	computational fluid dynamics

English symbols

C_D	drag coefficient
$C_{\varepsilon 1}$	empirical constant used in *k*-ε turbulence model
$C_{\varepsilon 2}$	empirical constant used in *k*-ε turbulence model
C_μ	empirical constant used in *k*-ε turbulence model
g	acceleration due to gravity
k	turbulent kinetic energy
L	length scale
p	fluid pressure
Re	Reynolds number
t	time
T_i	integral timescale
T_L	fluid Lagrangian integral time
U	mean velocity
x	axial co-ordinate
r	radial co-ordinate, equations (1)-(3)
u	axial velocity
v	radial velocity
r	random number, equation (22)

Greek symbols

α	under-relaxation factor
α_t	turbulent scaling factor
ε	dissipation rate of *k*
l	length scale
μ	dynamic viscosity
μ_τ	turbulent eddy viscosity
ν	kinematic viscosity
ρ	fluid density
σ_ε	empirical constant used in *k*-ε turbulence model
σ_κ	empirical constant used in *k*-ε turbulence model
τ_f	fluid time scale
τ_p	particle relaxation time
ζ	random number

Subscripts

$_p$	particle phase
$_r$	radius
$_t$	turbulent

Superscripts

$'$	fluctuating component
^{n}	time level

Special symbol

$\overline{\quad}$	ensemble average

1. Introduction

After a rapid growth in the number of nuclear power plants in P.R. China since the seventies, there are now eleven units in operation in three bases: Daya Bay, Qinshan and Tianwan. The current capacity of 660MW will be increased to 870MW after another four units start operating next year; the forecast capacity is 3600MW by 2020. However, plant safety is persistently called into question due to both political and economical pressures. One main concern is leakage from the primary system and, to counter this issue, a good detection system is desired for the in-service system. Several efforts are currently designed and evaluated for new nuclear reactors (Yadigaroglu and Dreier, 1998). In recent works, CFD techniques have been widely used to investigate flow fields in complex geometries (Orszag and Staroselsky, 2000; Tang, 1988), which meet the needs to quickly demonstrate a conceptual design without expensive experiments.

The present investigation concentrates on the problem of a dose diffusion pipe for releasing chemical test solutions or tracers into the cooling system of a model reactor in order to detect a leak from the primary system. The flow with tracers is considered a particle-laden flow. The flow through a constriction pipe is widely used in various applications and dispersed fluid-particle flows are encountered in a variety of industrial processes that are reviewed by Davies (2001). The design applications of constriction pipes include converging-diverging nozzles, orifice plates and junction units, among others. These normally have a constriction or expansion ratio from 2:1 to 4:1. The flow pattern is quite well known since many studies are available, both in experimental and numerical investigations for industrial applications (Szabo *et al*., 1997; Ahmed, 1998; Minota *et al*., 1998; Adamopoulos and Petropakis, 1999; Gruhn *et al*., 2000; Yang *et al*., 2000; Kunisch and Marduel, 2000; Lavante *et al*., 2001).

However, examples of dense particle flows through constrictions, expansion channels or particle laden jet flows are unusual (Marjanovic *et al*., 1999; Wapperom and Keunings, 2000), because these are difficult or expensive to measure experimentally. As a result, design applications of constriction pipes are limited, or rely heavily upon empiricism. Numerical simulation is sometimes the only quick way to obtain solutions for these unusual cases. Improvements were made on how the design can be simulated and many variations can be tested in order to arrive at the optimal design condition. The foresight gained from simulations helps to shorten the design process (Kunisch and Marduel, 2000; Trosset and Torczon, 1997). However, because of the limitation of numerical approaches, there are still challenges in the development of algorithms for the simulation of flows with fluid-particle and particle-particle interactions, named two-way and four-way momentum coupled methods.

Previous numerical simulations include the prediction of particle correlations with the continuous phase by Liao *et al*. (1997) and Lun (2000). Two-way coupled effects have been reviewed by Crow *et al*. (1996) and Kenning and Crow (1997), and are considered to be realistic for many industrial cases. Comprehensive reviews of Lagrangian Stochastic Monte-Carlo particle-tracking schemes are given in previous works by one of the authors (Barton, 1995; Morgan and Barton, 2000) for the investigation of various two-phase flow problems.

A numerical experiment was performed by using the commercial CFD package FLUENT (Fluent, 1998) to investigate the flow characteristics of the interaction between fluid and particles in a turbulence field through a 10:1 constriction pipe in the piping system of a model nuclear reactor. The simulations employed a Lagrangian Stochastic Monte-Carlo particle-tracking approach (Migdal and Agosta, 1969; Barton, 1999) and the averaged Reynolds equations with a k-ε turbulence model (Launder and

Spalding, 1974) with the two-layer zonal method (Chasnov and Tse, 2001; Guézengar *et al*., 1999). The present investigation includes a comparison of the flow field for the original conceptual design geometry and a modified design, as well as of the numerical strategy for solution of the two-way coupled flow. While experimental data are not available for comparison, the model predictions provide recommendations for a qualitative analysis of conceptual designs, and the results have proved useful for the optimisation of the geometry.

2. Flow Configuration

The flow configuration for the present computational study is shown in Fig. 1, with geometrical and fluid parameters indicated in this section. The three geometries are similar except for the structure of the constricting section. As shown in the figure, case 1 is designed with a long constriction section, case 2 has a round throat, while case 3 has a short round throat. The study considers a mixture of fluid and particles, where the mixture passes from the converging inlet with a diameter of 40 mm through a constriction with a diameter of 4 mm, which is located 40 mm downstream from the inlet, and finally to a diverging outlet, with the same diameter as that of the inlet, located 160 mm downstream from the inlet for case 1 and 170 mm for cases 2 and 3. The particles have a uniform diameter of 30μm. The particle-wall interactions are treated as "rebound" by a reflecting boundary. The continuous phase is air, with density 1.225 kg/m^3 and viscosity 1.7894×10^{-5} kg/m/s. The density of the particulate phase is 500 kg/m^3, appropriate to ash or similar tracer materials. The inlet void fraction is set to 5%, while the inlet velocity takes the values of 10m/s, 20m/s, and 30m/s. The flow is considered as axisymmetric. The present study only focuses on the

two-way coupled approach (particle-gas and particle-wall interaction), thus particle-particle interactions are neglected.

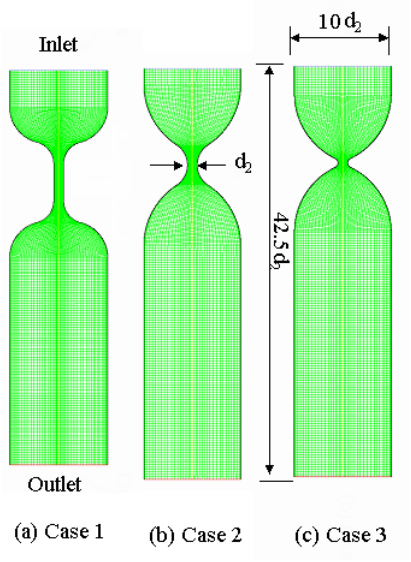

Fig.1 Geometries of computational domain.

3. Numerical Modelling of the Continuum Phase

The flow field is modelled using the averaged Reynolds equations with a standard k-ε turbulence model (Launder and Spalding, 1974), with the two-layer near-wall treatment. The governing equations are briefly described below.

3.1 Governing equations

The equation for conservation of mass, or continuity equation for axisymmetric geometries, can be written as follows:

$$\frac{\partial \rho}{\partial t} + \nabla \cdot \rho \vec{v} = 0 \qquad (1)$$

where ρ is the fluid density and $\nabla \cdot \vec{v} = \frac{\partial u}{\partial x} + \frac{\partial v}{\partial r} + \frac{v}{r}$, in which x is the axial coordinate, r is the radial coordinate, u is the axial velocity and v is the radial velocity. The momentum equations are given by

$$\frac{\partial}{\partial t}(\rho u)+\frac{1}{r}\frac{\partial}{\partial x}(r\rho uu)+\frac{1}{r}\frac{\partial}{\partial r}(r\rho vu)=-\frac{\partial p}{\partial x}+\frac{1}{r}\frac{\partial}{\partial r}\left[r\mu\left(\frac{\partial u}{\partial r}+\frac{\partial v}{\partial x}\right)\right]$$
$$+\frac{1}{r}\frac{\partial}{\partial x}\left[r\mu\left(2\frac{\partial u}{\partial x}-\frac{2}{3}(\nabla\cdot\vec{v})\right)\right] \quad (2)$$

$$\frac{\partial}{\partial t}(\rho v)+\frac{1}{r}\frac{\partial}{\partial x}(r\rho uv)+\frac{1}{r}\frac{\partial}{\partial r}(r\rho vv)=-\frac{\partial p}{\partial r}+\frac{1}{r}\frac{\partial}{\partial x}\left[r\mu\left(\frac{\partial u}{\partial r}+\frac{\partial v}{\partial x}\right)\right]$$
$$+\frac{1}{r}\frac{\partial}{\partial r}\left[r\mu\left(2\frac{\partial v}{\partial r}-\frac{2}{3}(\nabla\cdot\vec{v})\right)\right]-2\mu\frac{v}{r^2}+\frac{2}{3}\frac{\mu}{r}(\nabla\cdot\vec{v}) \quad (3)$$

where μ is the fluid viscosity and p is the pressure.

Turbulence effects are modelled by replacing the velocity and pressure in the above equations by the sum of their mean and fluctuating components. When time averages are applied a new group of terms, the Reynolds stresses, appear in the momentum equations. The averaged Reynolds equations closure problem is circumvented by applying Boussinesq's approximation, which assumes proportionality between the deviatoric part of the Reynolds' stress tensor and the strain tensor.

3.2 **Near wall treatment**

Near wall treatment for wall-bounded turbulence flows is employed by using the two-layer zonal approach (Chieng and Launder, 1980). In the two-layer model, the whole domain is subdivided into a viscosity-affected region and a fully developed turbulent region. The demarcation of the two regions is determined by a wall distance based on the turbulence Reynolds number, Re_y, defined as

$$\mathrm{Re}_y \equiv \frac{\rho\sqrt{k}\,y}{\mu} \quad (4)$$

where k is the kinetic energy.

In the fully turbulent region, the standard k-ε equations are employed (Launder and Spalding, 1974). In the viscosity-affected near-wall region, the one-equation model of Wolfstein (1969) is employed. The turbulent viscosity, μ_t, is computed from

$$\mu_t = \rho C_\mu \sqrt{k} l_\mu \tag{5}$$

while the rate of dissipation of kinetic energy ε is computed from

$$\varepsilon = \frac{k^{3/2}}{l_\varepsilon} \tag{6}$$

The length scales l_μ and l_ε in Eqs. (5) and (6) are computed from Chen and Patel (1988),

$$l_\mu = c_l y \left[1 + \exp\left(-\frac{\mathrm{Re}_y}{A_\mu} \right) \right] \tag{7}$$

$$l_\varepsilon = c_l y \left[1 + \exp\left(-\frac{\mathrm{Re}_y}{A_\varepsilon} \right) \right] \tag{8}$$

where $c_l = kC_\mu^{-3/4}$, $A_\mu = 70$, $A_\varepsilon = 2c_l$, $C_\mu = 0.09$ (Launder and Spalding, 1974).

When the two-layer zonal model is employed, y^+ at the wall-adjacent cell should ideally be of the order of $y^+=1$; however, an y^+ value less than 4~5 is acceptable as long as it is well inside the viscous sub-layer. The solution of the near-wall mesh is achieved using an adaptive mesh approach so that that the y^+ condition is satisfied.

3.3 **Numerical schemes**

The governing equations are solved by the finite volume method (Patankar, 1980) using the commercial CFD package FLUENT. The equations are integrated in space and time, using upwind differencing in space and implicit differencing in time. Each governing equation is linearised implicitly with respect to that equation's dependent variable. This results in a system of linear equations with one equation for each cell in the domain. The set of algebraic equations is solved by using a point implicit Gauss-Seidel linear equation solver in conjunction with an algebraic multigrid (AMG) method (Wesseling, 1992; Stüben, 2001). The calculation domain is divided into approximately 30 × 244 control volumes with grid refinement in the boundary layer in

the axial and radial directions. The grid is non-uniform in the axial and radial directions in order to have smaller control volumes close to the constriction and walls. This is illustrated in Fig. 2.

The grid dependence study is based on numerous refinements of the preliminary meshes and the final grid resolution gives adequate refinement. Meshes contained around 7320 cells without boundary layer refinement and about 12000~15000 cells when it is introduced.

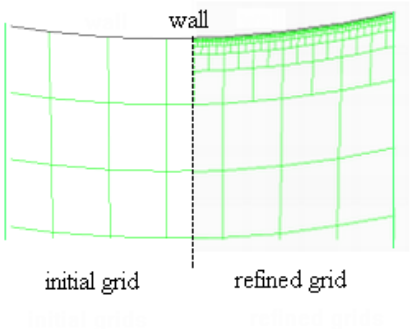

Fig.2 Near wall treatment.

4. The Particle Interaction Approach

The Lagrangian dispersed phase model (Migdal and Agosta, 1969) is used for the prediction of the trajectory of a particle phase based on previous work by one of the authors (Barton, 1999). In calculating the trajectories, the particles are assumed to be spherical and non-rotating. The force balance on each particle equates the particle inertia with the forces acting on it. For particles which are significantly denser than the fluid, the motion of the particles is assumed to be dominated by drag and gravity, and can be written as:

$$\frac{d\vec{u}_p}{dt} = F_D(\vec{u} - \vec{u}_p) + \vec{g}(\rho_p - \rho)/\rho_p + \vec{F}_{other} \qquad (9)$$

where $F_D(\vec{u} - \vec{u}_p)$ is the drag force per unit particle mass, with

$$F_D = \frac{18\mu}{\rho_P d_P^2} \frac{C_D \mathrm{Re}_p}{24} \tag{10}$$

$$\mathrm{Re}_p = \frac{\rho d_P \left| \vec{u}_P - \vec{u} \right|}{\mu} \tag{11}$$

where ρ_p is the particle density, d_p is the particle diameter, Re_p is the relative particle Reynolds number, $\vec{u}_p$ is the particle velocity, $\vec{u}$ is the fluid velocity, and C_D is the drag coefficient, given by:

$$C_D = a_1 + \frac{a_2}{\mathrm{Re}_p} + \frac{a_3}{\mathrm{Re}_p^2} \tag{12}$$

where the constants are given by Morsi and Alexander (1972) and take into account the ultra-Stokes drag.

Equation (9) incorporates additional forces in the particle force balance that can be important under special circumstances (Fluent, 1998). The first of these is the 'virtual mass' force, which is the force required to accelerate the fluid surrounding the particle. This force can be written as

$$\vec{F}_{other} = \frac{1}{2} \frac{\rho}{\rho_p} \frac{d}{dt} (\vec{u} - \vec{u}_p) \tag{13}$$

and is important when $\rho >> \rho_p$. An additional force arises due to the pressure gradient in the fluid:

$$\vec{F}_{other} = \frac{\rho}{\rho_p} \vec{u}_p \nabla \cdot \vec{u} \tag{14}$$

A stochastic tracking technique (Kuo, 1986; Bird, 1994) is used to take into account the effect of turbulent velocity fluctuations on the particle trajectories. In Eq. (9), the velocity term includes the instantaneous value of the fluctuating fluid velocity:

$$u = \overline{u} + u' \tag{15}$$

in order to predict the dispersion of the particle due to turbulence. By computing the trajectory in this manner for a sufficient number of representative particles, the random effects of turbulence on the particles can be modelled. By means of the discrete random walk model (Gosman and Ioannides, 1983; Tanaka *et al*., 1991), the fluctuating velocity components apply discrete piecewise constant functions with respect to time. Also, the random value is kept constant over an interval of time given by the characteristic lifetime of the eddies.

Prediction of particle dispersion makes use of the concept of the integral time scale, T, which describes the time spent in turbulence motion along the particle path *ds:*

$$T = \int_0^\infty \frac{u_p'(t)u_p'(t+s)}{\overline{u_p'^2}} ds \tag{16}$$

and is proportional to the particle dispersion rate. It can be shown that the particle diffusivity is given by $\overline{u_i'u_j'}T$. When particles move with the fluid, the integral time becomes the fluid Lagrangian integral time T_L, which can be approximated as:

$$T_L = C_L \frac{k}{\varepsilon} \tag{17}$$

where C_L is a constant to be determined which is generally not well known, although some proposed values have been reviewed by Barton (1995). By matching the diffusivity of tracer particles to the scalar diffusion rate predicted by the turbulence model, ν_t / σ, where ν_t is the turbulent viscosity and σ is the turbulent Prandtl number (Mostafa, 1992), the value of T_L becomes (Daly and Harlow, 1970):

$$T_L \approx 0.15 \frac{k}{\varepsilon} \tag{18}$$

In the stochastic discrete random walk model, the interaction of a particle with a succession of discrete stylised fluid phase turbulence eddies is simulated. Each eddy

is characterised by a Gaussian distributed random velocity fluctuation, $\vec{u'}$, and a time scale τ_e. The values of $\vec{u'}$ that prevail during the lifetime of the turbulent eddy obey a Gaussian probability distribution, e.g.

$$u' = \zeta\sqrt{\overline{u'^2}} \tag{19}$$

where ζ is a normally distributed random number between 0 and 1, and the remainder of the right-hand side is the local root mean square (rms) value of the velocity fluctuations. At each point in the flow, the value of the rms fluctuating components can be obtained from the kinetic energy as:

$$\sqrt{\overline{u'^2}} = \sqrt{\overline{v'^2}} = \sqrt{2k/3} \tag{20}$$

The lifetime of the eddy is defined as a random variation about T_L:

$$\tau_e = -T_L \log(r) \tag{21}$$

where r is a uniform random number between 0 and 1. The particle is assumed to interact with the fluid phase eddy over this eddy lifetime. When the eddy lifetime is reached, a new value of the instantaneous velocity is obtained by applying a new value of ζ in Eq. (19).

In Eq. (9), the fluid is time-averaged and is considered to be constant during a particle time step. In order to improve the accuracy of pathline calculation and particle trajectory calculation, the fluid phase velocity at the n+1 time level is approximated by

$$u^{n+1} = u^n + \Delta t \nabla u \cdot u_p^n \tag{22}$$

Results with and without the velocity gradient correction of Eq. (22) are compared in this paper. The technique of prediction and correction of the fluid velocity adopted here was explained in detail by Barton (1996). It is therefore expected that higher

accuracy of the continuous phase pathline and particle trajectory can be achieved with velocity gradient correction.

Due to the fact that the particles being simulated are inert and heat transfer is not significant, the only property transferred between the fluid and the particles is momentum. FLUENT keeps track of momentum gained or lost by particle streams that follow a certain trajectory, and this quantity is incorporated into the governing fluid equations and subsequent calculations. It is important to incorporate this two-way coupling since the mass loading of the flow is very high. The two-way coupling between particles and continuum is accomplished by alternately solving the particle and continuum phase equations until both solutions converge.

Momentum transfer is computed by examining the change in momentum of a particle as it passes through each control volume, which appears as a momentum sink in the continuum phase momentum balance:

$$F = \sum_{p=1}^{NCV} \left(\frac{18\mu C_D \operatorname{Re}_p}{24\rho_p d_p^2} \left(\vec{u}_p - \vec{u} \right) + F_{other} \right) \dot{m}_p \Delta t \tag{23}$$

where NCV is the number of control volumes, $\dot{m}_p$ is the particle mass flow rate, Δt is the time step, F_{other} represents other interactive forces.

When stochastic tracking is performed, the above inter-phase exchange term is computed for each stochastic trajectory with the particle mass flow rate $\dot{m}_p$ divided by the number of stochastic tracks computed. This implies an equal mass flow of particles follows each stochastic trajectory.

5. Results and Discussions

5.1 Solution Strategy

The results presented in Figures 3 to 26 are for two-way coupled flows where turbulence fluctuations affect the particle trajectories. The procedure of achieving

two-way coupled flow simulations in the present investigation, based on FLUENT, is to get a converged solution of the continuous phase flow field by performing the following tasks:

- Introduce the particle phase, calculating the particle trajectories for the injection.
- Resolve the continuous phase field, using the interphase exchange.
- Recalculate the particle trajectories in the modified continuous phase flow field.
- Repeat the previous two steps until a converged solution is achieved.

It is important to consider the convergence criteria, under-relaxation factors and the ratio of the particle phase iteration to the fluid calculations. The following possible strategies can be adopted: (a) increase under-relaxation factors of particle phase, (b) decrease under-relaxation factors of continuous phase, (c) set up the number of continuous phase calculations per particle phase iteration to a low number (typically less than 3).

Here we take the following steps to accelerate convergence:

(1) Increase the convergence criteria at each step or switch off convergence checking.

(2) Decrease the convergence criteria or keep it switched off and reduce under-relaxation factors temporarily.

(3) Set up a number of continuous phase iterations per particle phase iteration, i.e., 100.

(4) Set up a sufficient number of stochastic calculations, greater than 50.

(5) Set up a monitor surface to check the variation of a particular variable with iterations. In this study, we monitor the mean velocity in the throat.

(6) Check that the number of steps for the applied tracking is sufficient to avoid incomplete particle tracking within the domain.

Despite these strategies, we should emphasize that there are difficulties in achieving convergence. This is a challenging procedure, especially as it appears to be case sensitive.

5.2 **Results and Discussions**

The simulations for dispersion of particles from a uniform concentration profile at the inlet of the channel are described in this section. The flow patterns show the difference between the results for one-way and two-way coupling. Three geometry designs are compared for particle concentration, momentum exchange, velocity profiles, stream function, shear rate, turbulent kinetic energy, and other variables. The gravitational effect is neglected in these simulations. It is observed that particle flows affect the continuous phase flow in all three cases, and modifying the throat shape also affects the behaviour of the flows. The discussions first consider case 2, as it has more common features observed in the other two cases.

For case 2, velocity contours depicted in Fig. 3 show that there is a maximum velocity of the continuous phase flow field located at the minimum diameter section. Comparing velocity results for the one-way and two-way coupled flow patterns shown in Fig. 3 and Fig. 4, two-way coupled flows have a higher velocity magnitude due to the drag and inertia forces of the particles, which will increase the velocity magnitude of the gas phase as described in Eq. (23). However, the particles in the two-way coupled flow only affect the flow downstream of the constriction, and upstream of the constriction similar flow fields are observed. The velocities along the axis for three different inlet velocities are shown in Fig. 5, which also indicate that the maximum velocity is located in the throat.

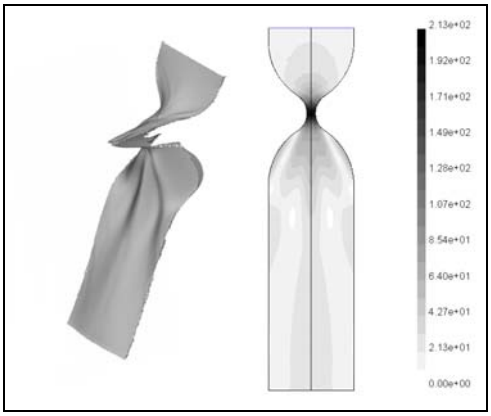

Fig.3 Right: Velocity contours in two-way coupled flow, Case 2, inlet velocity 20m/s. Left: 3D graphical display.

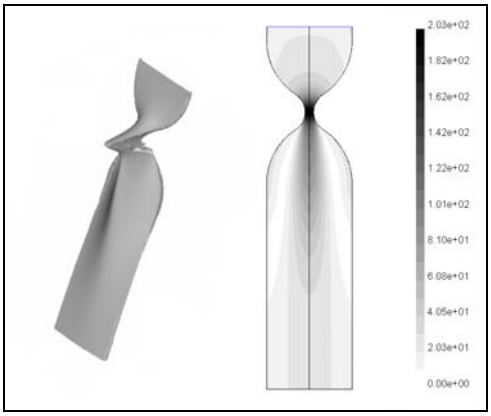

Fig.4 Right: Velocity contours in one-way coupled flow, Case 2, inlet velocity 20m/s. Left: 3D graphical display.

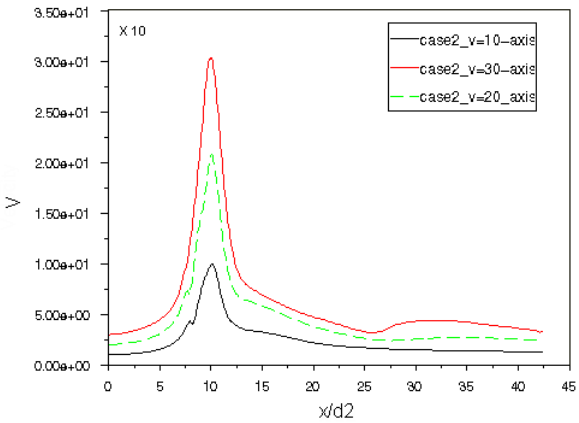

Fig.5 Axial velocity, Case 2, inlet velocities 10m/s, 20m/s, 30m/s.

The flow separation in the diverging section is shown in Fig. 6. The size of the recirculating region for one-way coupled flows is bigger than for two-way coupled

flows, as shown on the right graph of Fig. 6. This is because two-way coupling includes a term accounting for momentum interphase exchange, shown in Fig. 7, which increases from velocity 10m/s to 30m/s. The shear rate also increases with increasing inlet velocity (Fig. 8). The fluctuation of shear rates is larger in two-way coupled flows than in one-way coupled flows (Fig. 9).

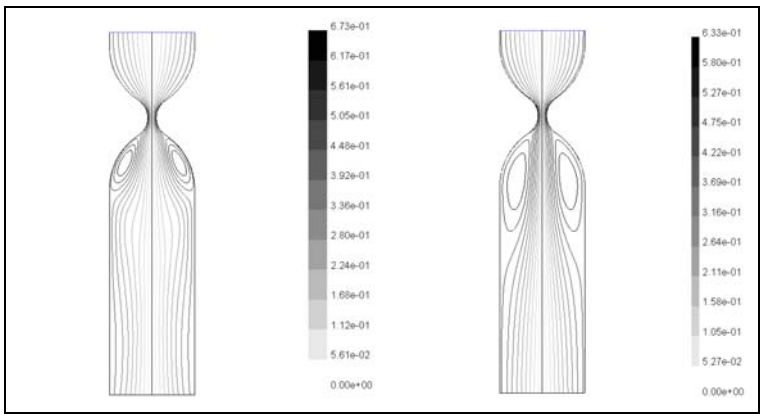

Fig.6 Streamline contours in two-way coupled flow (left) and in one-way coupled flow (right), Case 2, inlet velocity 20m/s.

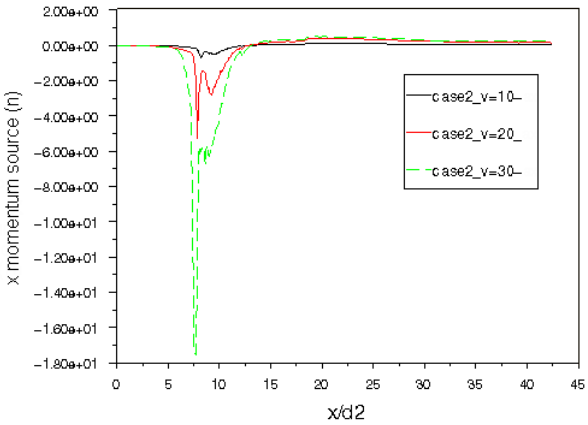

Fig.7 Interphase exchange of momentum source along the *x*-axis, Case 2, inlet velocities 10m/s, 20m/s, 30m/s.

The normalised concentration scales of particles distribution are defined between maximum and minimum concentration values in order to show a relative comparison. The results are shown in Figs. 10 and 11. The maximum value is located at the entrance to the throat due to the effects of particle–wall interaction, where particles rebound and increase the local concentration. This causes a build-up at the front of the

throat. It is expected that the wall of the converging part will suffer wear or erosion problems, and the numerical results show the location where particle-wall collision may occur. Special measures regarding the surface or wall thickness could be taken to avoid wear or erosion, and modifying the throat shape will avoid particle agglomeration.

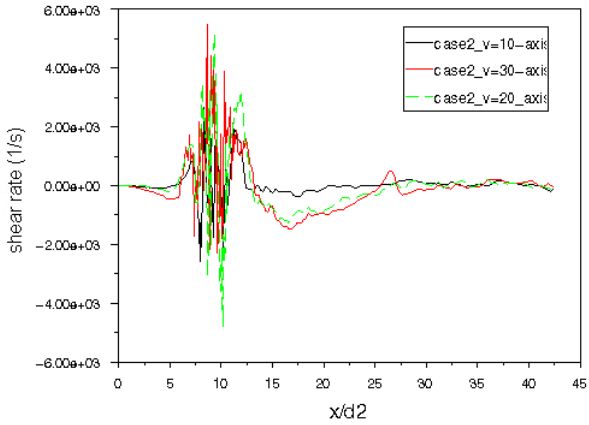

Fig.8 Axial shear rate, Case 2, inlet velocities 10m/s, 20m/s, 30m/s.

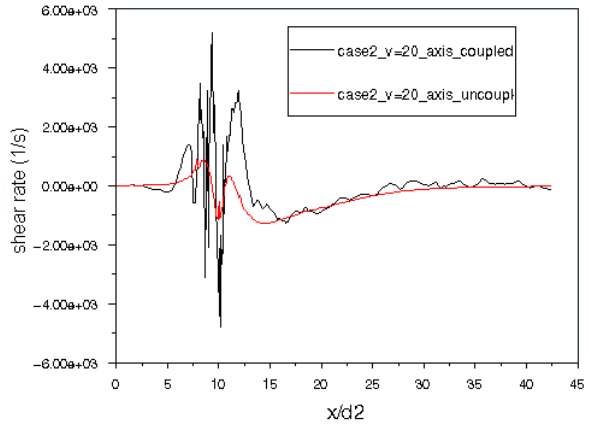

Fig.9 Axial shear rate in two-way coupled and one-way coupled flows, Case 2, inlet velocity 20m/s.

Velocity profiles are shown in Figs. 12 and 13, indicating the fluctuations of velocity due to two-way coupled flows at profile positions x = $12.5d_2$, $15.3d_2$, and $22.5d_2$. Comparing the velocity profiles shown in Figs. 12 and 13, this influence decreases for the higher inlet velocity in Fig. 13. The profiles appear smooth, which

indicate that the effects of two-way coupling on the continuous phase are less than in the lower velocity case.

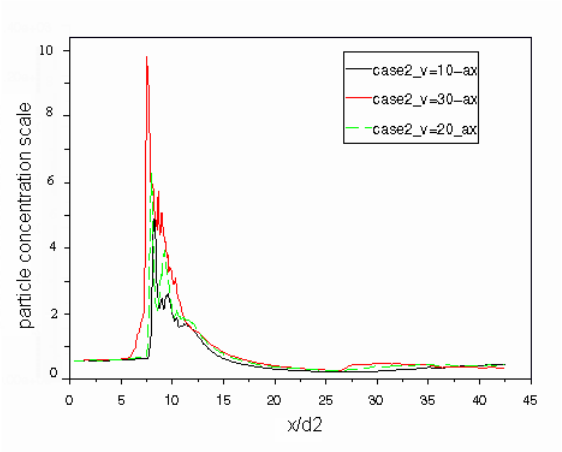

Fig.10 Particle concentration scale along the *x*-axis, Case 2, inlet velocities 10m/s, 20m/s, 30m/s.

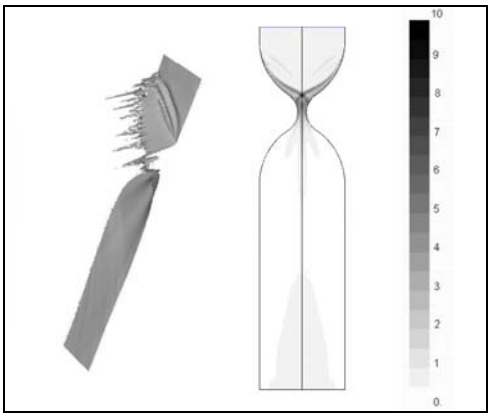

Fig.11 Right: Concentration contours of particle distribution, Case 2, inlet velocity 20m/s. Left: 3D graphical display (left half).

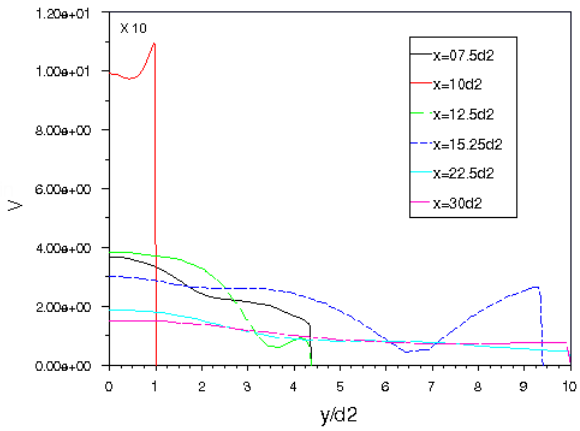

Fig.12 Velocity profiles at x = 7.5d_2, 10 d_2, 12.5 d_2, 15.25 d_2, 22.5 d_2, 30 d_2, Case 2, inlet velocity 10m/s.

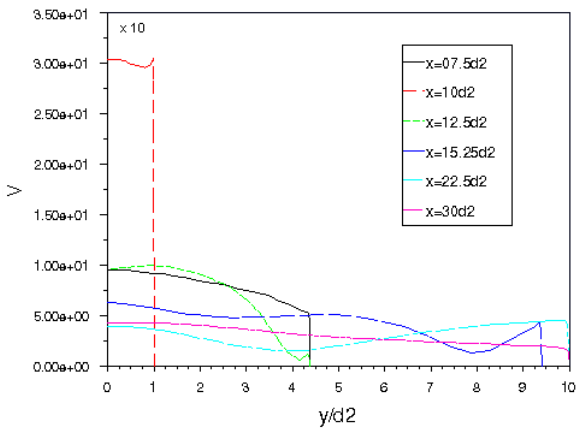

Fig.13 Velocity profiles of at x = 7.5d_2, 10 d_2, 12.5 d_2, 15.25 d_2, 22.5 d_2, 30 d_2, Case 2, inlet velocity 30m/s.

Case 1 has similar features to case 2, but the size of the recirculation region is bigger than case 2 for the same inlet velocity, for both one-way and two-way coupled flows, as shown in Fig. 14. As the fluid accelerates in the long constriction section, it comprises jet-like flow features. The normalised concentration scale of particle distribution shown in Figs. 15 and 16 causes a significant build-up in front of the throat due to the abrupt change. The momentum exchange between the particle phase and the fluid phase occurs mainly in front of the throat (Fig. 17). The velocity profiles reveal heavy velocity fluctuation by the particle phase even far downstream of the constriction, as in section x=30d_2 depicted in Fig. 18. The two sharp changes of shear rate are easily identified in Fig. 19, which coincide with entrance and exit of the constriction.

The flow characteristics of case 3 are also similar to case 2. The minimum size of the two recirculating regions appears for inlet velocity of 20m/s (Fig. 20), while the maximum size appears for 30m/s (Fig. 21). It seems that there is a critical velocity for the formation of the minimum size of the recirculation region. Since the structure of the throat is a small round radius, which induces a zone behind the throat for

expansion of the flow, the recirculation regions are strongly dependent on the accelerated flow near walls as illustrated in Figs. 22 and 23.

The velocity profiles reveal that the fluctuations of the velocity at the downstream locations are smooth, as shown in Figs. 22 and 23. This means that the flow is more homogeneous than in cases 1 and 2, as depicted in Figs.12, 13 and 18. This feature could be important in some design applications especially for mixing processes in the food, dairy, and biochemical industries, e.g. to avoid vibration/swing of the piping due to velocity fluctuations.

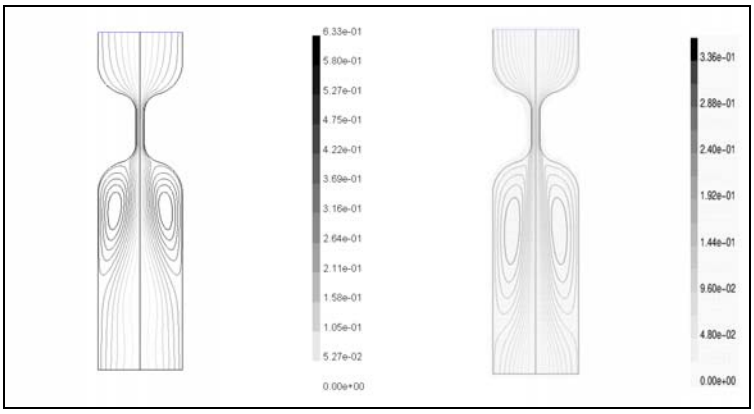

Fig.14 Streamline contours in two-way coupled flow (left) and in one-way coupled flow (right), Case 1, inlet velocity 10m/s.

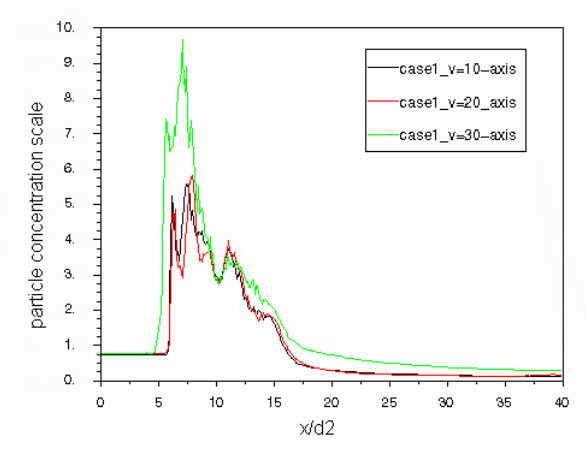

Fig.15 Particle concentration scale along the *x*-axis, Case 1, inlet velocities 10m/s, 20m/s, 30m/

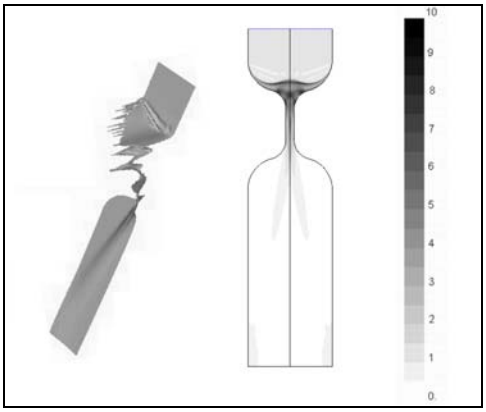

Fig.16 Right: Concentration contours of particle distribution, Case 1, inlet velocity 20m/s. Left: 3D graphical display (left half).

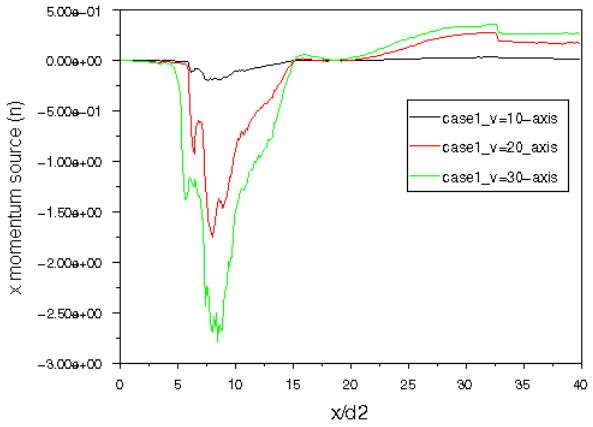

Fig.17 Interphase exchange of momentum source along the *x*-axis, Case 1, inlet velocities 10m/s, 20m/s, 30m/s.

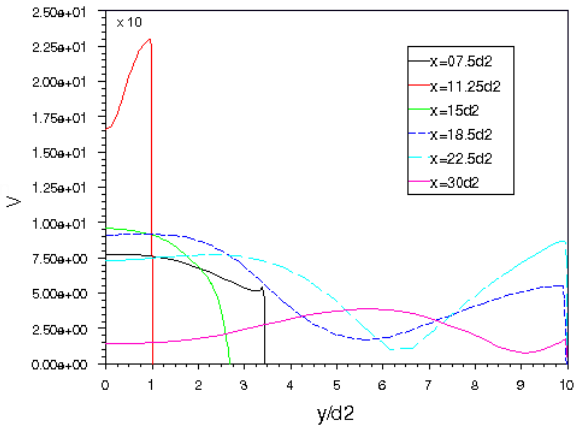

Fig.18 Profiles of velocity at $x = 7.5d_2$, 11.25 d_2, 15 d_2, 18.5 d_2, 22.5 d_2, 30 d_2, Case 1, inlet velocity 20m/s.

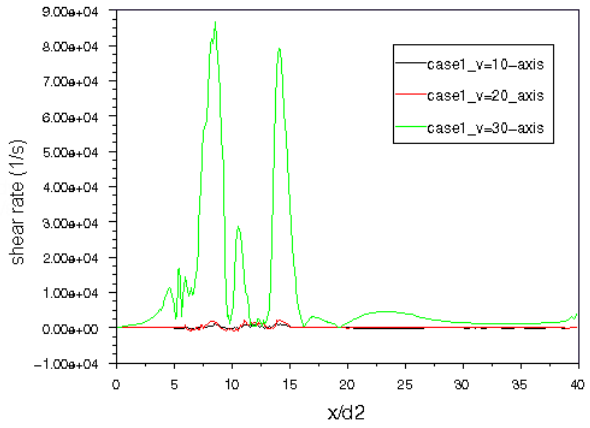

Fig.19 Axial shear rate, Case 1, inlet velocities 10m/s, 20m/s, 30m/s.

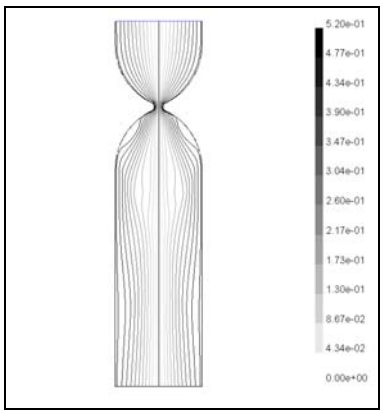

Fig.20 Streamline contours, Case 3, inlet velocity 20m/s.

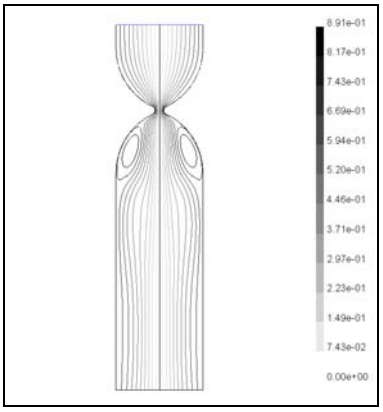

Fig.21 Streamline contours, Case 3, inlet velocity 30m/s.

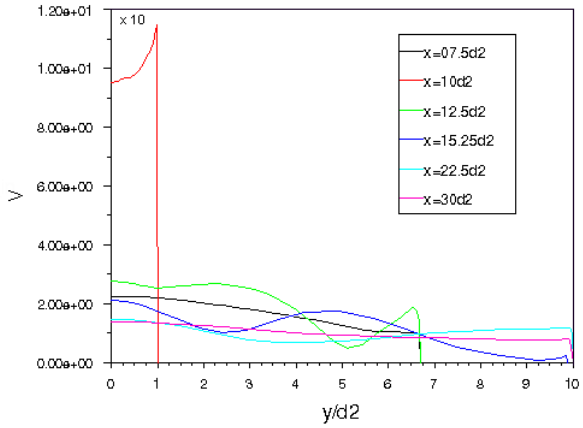

Fig.22 Profiles of velocity at x = 7.5d_2, 10 d_2, 12.5 d_2, 15.25 d_2, 22.5 d_2, 30 d_2, Case 3, inlet velocity 20m/s.

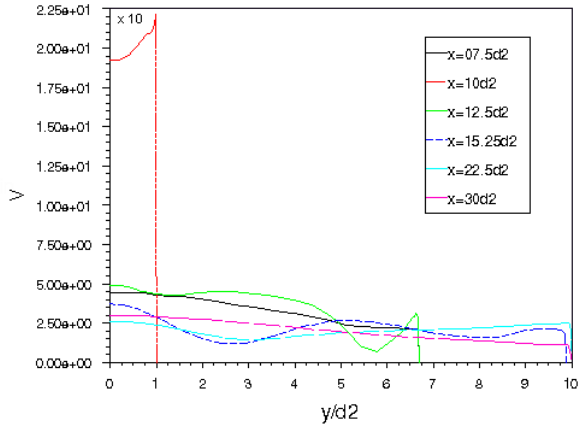

Fig.23 Profiles of velocity at x = 7.5d_2, 10 d_2, 12.5 d_2, 15.25 d_2, 22.5 d_2, 30 d_2, Case 3, inlet velocity 20m/s.

5.3 **Overview**

The particle interactions affect the flow of the continuous phase computed by the two-way momentum coupling method. The fluctuations of the velocity at the downstream locations are smoother along the axis from cases 1 to 3 (Fig. 24). The interphase exchange of momentum source is stronger from cases 1 to 3 (Fig. 25). The differences between the particle trajectories and pathlines are compared by employing the velocity gradient correction with Eq. (22). Comparing pathlines with and without the velocity gradient correction in two-way coupled flows, it is observed that the vortex has a smaller size with the velocity gradient correction (Fig. 26). It is noted that

the velocity gradient correction plays a significant factor for the accuracy of the particle trajectories and pathlines in the two-way coupling approach.

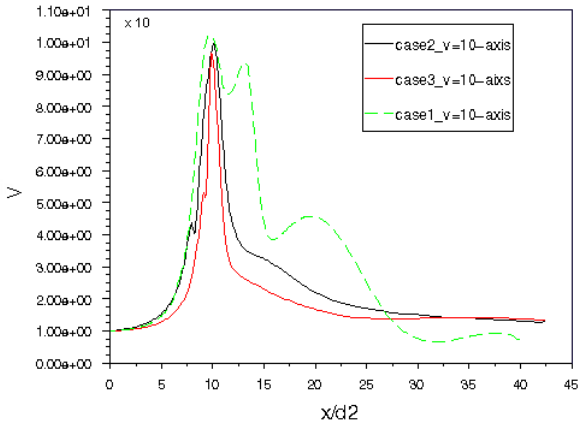

Fig.24 Axial velocity profiles, inlet velocity 10m/s, Cases 1, 2, and 3.

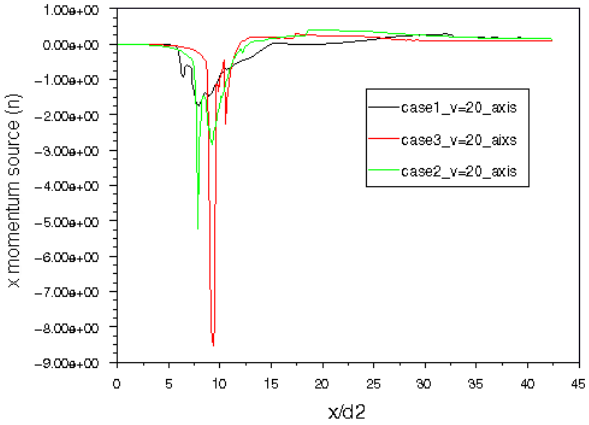

Fig.25 Interphase exchange of momentum source along the *x*-axis, inlet velocity 20m/s, Cases 1, 2 and 3.

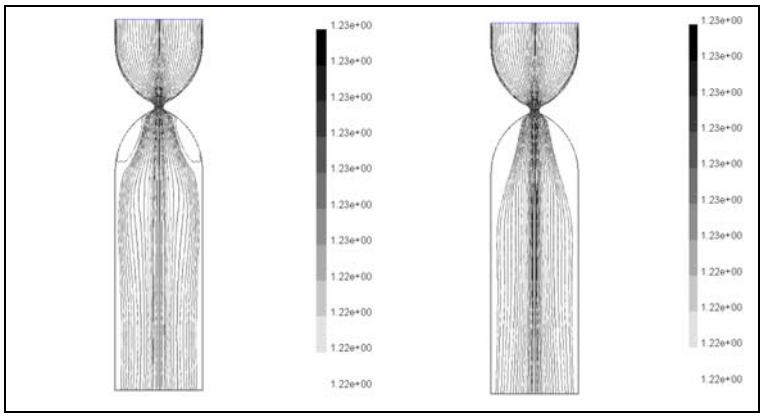

Fig.26 Velocity pathlines in two-way coupled flow with velocity gradient correction (left) and without velocity gradient correction (right), Case 3, inlet velocity 10m/s.

5.4 **Summary**

The numerical experiments are performed for a special diffusion pipe design since there is increasing need to be able to control dose dispersion flow field and hence, an improved capability to numerically simulate and study these processes. Numerical simulations are, in principle, ideally suited to study these flows and provide an insight into the process that is time consuming and expensive by experiments. The following remarks can be drawn:

(1) For the flow patterns in Figs. 6 and 14, coupled calculations show that the flow features of continuous phase fields are impacted by particle flow, and the vortex in the two-way coupled flow field is smaller than that in the one-way coupled flow field. The difference shows that particle interaction cannot be neglected.

(2) For the three geometries considered, the velocity profiles at the downstream section show that the flow fields are more homogeneous from cases 1 to 3, the profiles are smoother and the variable range is narrower. In view of design optimisation, this flow feature could be applied to improve the mixing process by using a different throat structure.

(3) It is observed that the size of the vortex increases with the inlet velocity in case 1, but decreases in case 2. However, the minimum size of vortex in case 3 appears at a velocity of 20m/s.

(4) Particles rebound causing inhomogeneous particle concentrations in front of the throat, and the particle trajectories are mainly outside of the vortex region in the rear position of throat.

(5) The prediction and correction of the fluid velocity is employed for improving accuracy of the particle interaction. It is observed that the formula for velocity

gradient correction impacts on the results of pathline calculations as well as particle trajectory calculations.

(6) The predictions show that the optimisation of the geometry can be based on the results of numerical investigations. The effect of modifying the structure can be easily tested through numerical simulations.

6. Conclusions

A numerical investigation is carried out for turbulent particle-laden flow through a dose diffusion pipe for a model reactor system. A Lagrangian Stochastic Monte-Carlo particle-tracking approach and the averaged Reynolds equations with a k-ε turbulence model, with the two-layer zonal method in the boundary layer, are used for the disperse and continuous phases. The flow patterns coupled with the particle dynamics are predicted. It is observed that the two-way coupling of the disperse and continuous phases is important in this case. It was found that the structures of the throat have significant effects on the particle distribution, flow patterns and size of the recirculation region. The accuracy of the simulations depends on the prediction and correction of the fluid phase velocity during the particular time interval. A numerical solution strategy for the computation of two-way coupled flow is discussed. All three cases have different flow features in the formation of a vortex behind the throat. This will be useful for the qualitative analysis of conceptual designs, and the results have proved useful for the optimisation of the geometry.

Acknowledgements

Financial support from EPSRC and the Mechanical Engineering Department at Brunel University is gratefully acknowledged. The authors would also like to thank the two anonymous referees for many helpful comments.

References

Adamopoulos, K.G.,Petropakis, H.J.,1999. Simulation of discrete inert particles in two phase supersonic mixing. Journal of Food Engineering 42, 59-66.

Ahmed, S.A., 1998. An experimental investigation of pulsatile flow through a smooth constriction. Experimental Thermal and Fluid Science 17, 309-318.

Barton, I.E. 1999. Simulation of particle trajectories in turbulent flow over a backward-facing step. R&D Journal 15, 65-78.

Barton, I.E., 1995. A numerical investigation of incompressible dilute particulate flow. Ph.D. Thesis. University of Manchester.

Barton, I.E., 1996. Exponential-Lagrangian tracking schemes applied to Stokes law. Journal of Fluids Engineering. Transaction of the ASME 118, 85-89.

Bird, G.A., 1994. Molecular Gas Dynamics. Clarendon Press, Oxford.

Chen, H.C., Patel, V.C., 1988. Near-wall turbulence models for complex flows including separation. AIAA journal 26, 641-648.

Chieng, C.C. Launder, B.E., 1980. On the calculation of turbulence heat transport downstream from an abrupt pipe expansion. Numer. Hear Transfer 3, 189-207.

Crow, C.T., Troutt, T.R., Chung, N., 1996. Numerical models for two-phase turbulent flows. Annual Rev. Fluid Mech. 28, 11-43.

Daly, B.J., Harlow, F.H., 1970. Transport equations in turbulence. Phys. Fluids 13, 2634-2649.

Davies, R., 2001. Particle science and technology –a view at the millennium. Powder Technology 119, 45-57.

FLUENT Documentation (User's guide, UDF manual, Text command list) version 5, Fluent Inc, Lebanon, NH, 1998.

Gosman A.D., Ioannides, E., 1983. Aspects of computer simulation of liquid-fuelled combustors. J. Energy **7,** 482–490.

Gruhn, P. Henckels, A. Kirschstein, S.,2000. Flap contour optimization for highly integrated SERN nozzles. Aerospace Science and Technology 4, 555-565.

Kenning, V.M., Crow, C.T., 1997. On the effect of particle on carrier phase turbulence in gas-particle flows. Int. J. Multiphase Flow 23, 403-408.

Kunisch, K., Marduel, X., 2000. Optimal control of non-isothermal viscoelastic fluid flow. Journal of Non-Newtonian Fluid Mechanics 88. 261-301.

Kuo, K.K-Y., 1986. Principles of Combustion. Wiley Interscience, p573-587.

Launder, B.E., Spalding, D.B., 1974. The numerical computation of turbulence flows. Comput. Meth. App. Mech. Engng. 3, 267-289.

Lavante, E. von, Zachcial, A., Nath, B., 2001. Dietrich, H., Unsteady effects in critical nozzles used for flow metering. Measurement 29, 1-10.

Liao, C.M., Lin, W.Y., Zhou, L.X., 1997. Simulation of particle-fluid turbulence interaction in sudden-expansion flows. Powder Technology 90, 29-38.

Lun, C.K.K., 2000. Numerical simulation of dilute turbulent gas-fluid flows. Int. J. Multiphase Flow 26, 1707-1736.

Marjanovic, P., Levy, A., Mason, D.J., 1999. An investigation of the flow structure through abrupt enlargement of circular pipe. Powder Technology 104, 296-303.

Migdal, D., Agosta, D.V., 1967. A source flow model for continuum gas-particle flow. Trans. ASME J. Appl. Mech. 34E, 860.

Minota, T., Nishida, M., Lee, M.G., 1998. On collision of two compressible vortex rings. Fluid Dynamics Research 22, 43-60.

Morgan, A.J., Barton, I.E., 2000. Comparison of Lagrangian tracking schemes for flow over a backward facing step. Communications in Numerical Methods in Engineering 16, 831-837.

Morsi, S.A., Alexander, A.J., 1972. An investigation of particle trajectories in two-phase flow systems. J. Fluid Mech. 55, 193-208.

Mostafa, A.A., 1992. Turbulent diffusion of heavy particles in turbulent jets. Journal of Fluid Engineering 8, 667-671.

Orszag, S.A. and Staroselsky, I., 2000. CFD: Progress and problems, Computer Physics Communications, 127, 165-171.

Patankar, S.V., 1980. Numerical Heat Transfer and Fluid Flow. Hemisphere Publishing Corporation, Taylor & Francis Group, New York.

Stüben, K., 2001. A review of algebraic multigrid methods. Journal of Computational and Applied Mathematics 128, 281-309.

Szabo, P.,Rallison, J.M.,Hinch, E.J., 1997. Start-up of flow of a FENF-fluid through a 4:1:4 constriction in a tube. Journal of Non-Newtonian Fluid Mech. 72, 73-86.

Tanaka, T., Kiribayashi, K., Tusji, Y., 1991. Monte Carlo simulation of gas-solid flow in vertical pipe or channel, In: Proc. Int. Conf. on Multiphase Flows, Tsukuba, Japan, vol. **2**, 439-442.

Tang, H., 1988. Numerical prediction of the 3-D step flow in near surface field. Proceedings of 4th National Conference on Structures of Nuclear Reactors, P.R. China.

Trosset, M.W., Torczon, V., 1997. Numerical Optimization Using Computer Experiments. NASA CR-201724, ICASE Report No. 97-38.

Wapperom, P., Keunings, R., 2000. Simulation of linear polymer melts in transient complex flow. Journal of Non-Newtonian Fluid Mech. 95, 67-83.

Wesseling, P., 1992. An Introduction to Multigrid Methods. John Wiley & Sons Ltd., England.

Wolfstein, M., 1969. The velocity and temperature distribution of one-dimensional flow with turbulence augmentation and pressure gradient. Int. J. Heat Mass Transfer 12, 301-318.

Yadigaroglu, G., Dreier, J., 1998. Passive advanced light water reactor designs and the LAPHA program at the Paul Scherrer Institute. Kerntechnik 63, 39-46

Yang, J., Jaenicke, R., Dreiling, V., Peter, T., 2000. Rapid condensational growth of particles in the inlet of particle sizing instruments. Journal of Aerosol Science 31, 773-788.